



HAL
open science

A Non-Aqueous Asymmetric Cell with a Ti₂C-Based Two-Dimensional Negative Electrode

Jérémy Come, M. Naguib, Patrick Rozier, M. W. Barsoum, Y. Gogotsi, Pierre-Louis. Taberna, Mathieu Morcrette, Patrice Simon

► **To cite this version:**

Jérémy Come, M. Naguib, Patrick Rozier, M. W. Barsoum, Y. Gogotsi, et al.. A Non-Aqueous Asymmetric Cell with a Ti₂C-Based Two-Dimensional Negative Electrode. *Journal of The Electrochemical Society*, 2012, 159 (8), pp.A1368-A1373. 10.1149/2.003208jes . hal-00821063

HAL Id: hal-00821063

<https://hal.science/hal-00821063>

Submitted on 19 Feb 2019

HAL is a multi-disciplinary open access archive for the deposit and dissemination of scientific research documents, whether they are published or not. The documents may come from teaching and research institutions in France or abroad, or from public or private research centers.

L'archive ouverte pluridisciplinaire **HAL**, est destinée au dépôt et à la diffusion de documents scientifiques de niveau recherche, publiés ou non, émanant des établissements d'enseignement et de recherche français ou étrangers, des laboratoires publics ou privés.



Open Archive Toulouse Archive Ouverte (OATAO)

OATAO is an open access repository that collects the work of Toulouse researchers and makes it freely available over the web where possible

This is an author's version published in: <http://oatao.univ-toulouse.fr/21780>

Official URL: <https://doi.org/10.1149/2.003208jes>

To cite this version:

Come, Jérémy^{ORCID} and Naguib, Michael and Rozier, Patrick^{ORCID} and Barsoum, Michel W. and Gogotsi, Yury and Taberna, Pierre-Louis^{ORCID} and Morcrette, Mathieu and Simon, Patrice^{ORCID} *A Non-Aqueous Asymmetric Cell with a Ti₂C-Based Two-Dimensional Negative Electrode*. (2012) *Journal of The Electrochemical Society (JES)*, 159 (8). A1368-A1373. ISSN 0013-4651

Any correspondence concerning this service should be sent to the repository administrator: tech-oatao@listes-diff.inp-toulouse.fr

A Non-Aqueous Asymmetric Cell with a Ti₂C-Based Two-Dimensional Negative Electrode

J. Come,^{a,b} M. Naguib,^{c,*} P. Rozier,^{a,b} M. W. Barsoum,^c Y. Gogotsi,^c P.-L. Taberna,^{a,b} M. Morcrette,^{b,d} and P. Simon^{a,b,**,z}

^a Université Paul Sabatier, CIRIMAT UMR CNRS 5085, 31062 Toulouse Cedex 4, France

^b Réseau sur le Stockage Electrochimique de l'Energie (RS2E), FR CNRS 3459, France

^c Department of Materials Science and Engineering, Drexel University and A.J. Drexel Nanotechnology Institute, Philadelphia, Pennsylvania 19104, USA

^d Laboratoire de réactivité et de Chimie des Solides, Université de Picardie Jules Verne, 80000 Amiens, France

A new *MXene* phase, Ti₂C, obtained by aluminum extraction from Ti₂AlC and exfoliation of the reaction product, was electrochemically studied vs. Lithium. Li-ions insertion into the 2-D structure was characterized by in situ XRD measurements. Additional electrochemical kinetic characterizations of Ti₂C, using a cavity micro-electrode, showed that the electrochemical reactions involve two different phenomena: one diffusion-limited, the other not. A Ti₂C/activated carbon asymmetric cell was assembled to highlight the high rate performance of the *MXene*. The cell was cycled between 1.0 V and 3.5 V, and showed good capacity retention during 1000 galvanostatic charge/discharge cycles at rates up to 10C.

[DOI: 10.1149/2.003208jes]

Among energy storage devices, electrochemical double layer capacitors (EDLCs) and Li-ion batteries (LIBs) are considered to be the best in terms of performance, durability and safety.^{1,2} LIBs possess energy densities of up to 200 Wh · kg⁻¹ but at the expense of limited power capability and cyclability.² EDLCs, on the other hand, are characterized by power densities of more than 10 kW · kg⁻¹, for a quasi-infinite number of charge/discharge cycles,^{3,4} EDLCs however, suffer from low energy densities (~5 Wh · kg⁻¹), because they are limited by the charge storage at active materials' surface. As a result, tremendous efforts are currently being devoted for increasing the energy density of supercapacitors, defined as:

$$E = \frac{1}{2} \cdot C_{dl} \Delta V^2 \quad (1)$$

where E is the energy (J), C_{dl} is the double layer capacitance (F) and ΔV is the operating voltage (V). Tailoring novel carbon nanostructures,⁵⁻⁷ matching ion size with pore size,⁸⁻¹¹ using pseudocapacitive materials with fast surface redox reactions,¹²⁻¹⁵ and increasing the voltage window using ionic liquid electrolytes^{9,16} are ways being explored to improve EDLCs' performance.

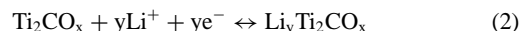
Non-aqueous asymmetric electrochemical capacitors have been proposed as an alternative way to overcome the low energy density of conventional EDLCs.^{3,17-21} This technology is based on the association of two materials involving distinct charge storage mechanisms, namely an activated carbon capacitive electrode and a Li-ion insertion faradaic electrode, both immersed in an organic electrolyte. Amatucci and *et. al.*¹⁷ were the first to demonstrate that such devices possess higher power densities than LIBs, while showing higher energy densities than EDLCs. They used nanocrystalline lithiated titania (LTO) as the active negative electrode and activated carbon as the positive electrode. The cell was cycled between 1.5 V and 3.0 V in an acetonitrile electrolyte up to a rate of 50C relative to LTO, and was able to deliver 25 Wh · kg⁻¹, with excellent cycling stability. JM Energy commercializes a 3.8 V carbon graphite/activated carbon asymmetric cell exhibiting 10 Wh · kg⁻¹ of packaged cell.¹⁸ Commercially available Li-ion capacitors have gravimetric energy densities of about 20 Wh · kg⁻¹, which is about three times higher than that of conventional carbon/carbon EDLCs.¹⁹ These results opened the door to a wide choice of Li ions insertion materials exhibiting high performance rates.

Obviously the choice of the faradaic electrode is of highest importance since it sets the kinetics and rate performance of the cell. Herein we report results on the design of a non-aqueous asymmetric

cell - based on a new two-dimensional (2-D) transition metal carbide material as the negative electrode, combined with a positive electrode of activated carbon, operating between 1.0 and 3.5 V.

Recently, 2-D nanocrystals of transition metal carbides were synthesized by exfoliation of ternary carbides with a $M_{n+1}AX_n$ formula, where M is an early transition metal, A is an A-group element and X is carbon and/or nitrogen, so-called *MAX* phases.²² The exfoliation process was carried out by selective etching the A layer using hydrofluoric acid, HF, at room temperature and ending up with 2-D layers of $M_{n+1}X_n$. We labeled these new phases *MXene* to emphasize the loss of A from *MAX*, and their similarity to graphene. The material of interest in this study is obtained by the exfoliation of Ti₂AlC. The post-exfoliation material obtained contained oxygen, hydroxide and fluoride groups at the surface of the Ti-layers.²³ Hence, the formulae of the material is assumed to be Ti₂CO_xH_yF_z, and will henceforth be referred to as Ti₂C for convenience, keeping in mind that oxygen/OH/F surface groups are present.

More recently, *MXene* showed promising performance as an anode material in LIBs.²⁴ Ti₂C was used in that study vs. lithium; the electrochemical Li⁺ ions insertion gave stable capacities of 160 mAh · g⁻¹ at C/10 rate and 70 mAh · g⁻¹ at 10C rate for more than 200 cycles. It was proposed that the lithiation and delithiation reaction was:



Experimental Details

The Ti₂C powders were obtained by immersing commercially purchased - 325 mesh, Ti₂AlC powders (3-ONE-2, Voorhees, NJ, > 92 wt.% purity) in 10% HF (Fisher Scientific, Fair Lawn, NJ) for 10 h at room temperature, as described elsewhere.²⁵ The obtained Ti₂C material was subsequently mixed with carbon black (TimCal super C65) and polyvinylidene fluoride (PVDF) binder in a 80:10:10 weight ratio in acetone. The slurry was then cast onto a copper foil current collector, from which 12 mm diameter disks were punched.

The electrode loading was comprised of between 2.5 and 3.5 mg · cm⁻². Commercially available microporous activated carbon powder (YP17 Kuraray Chemical Co., LTD, Japan) - obtained from carbonization of coconut shell⁹ - with a specific surface area of 1700 m² · g⁻¹ was used as positive electrode. The powder was mixed with 5 wt.% polytetrafluoroethylene (PTFE) binder (60 wt.% in H₂O, Aldrich) in ethanol. The paste was cold rolled and 14 mm diameter disks were punched. The mass loading was then adjusted depending on the negative active material mass. The freestanding electrode was placed onto a carbon-treated aluminum current collector to decrease the contact resistance.²⁶ Finally, the electrodes were dried at 120°C in vacuum for 12h.

*Electrochemical Society Student Member.

**Electrochemical Society Active Member.

^zE-mail: simon@chimie.ups-tlse.fr

Two-electrode CR2016 coin cells, and three-electrode nylon Swagelok cells consisting of a Ti_2C negative electrode and an activated carbon positive electrode separated by a glass fiber separator (Whatman, GF/A) saturated with 1M LiPF_6 in ethylene carbonate (EC) and dimethyl carbonate (DMC) 1:1 electrolyte (LP30, Merck) were tested. For the three-electrode cells, a Li metal foil was used as the reference.

High rate electrochemical kinetic characterizations were performed using a cavity microelectrode (CME) obtained from the French network “CNRS microelectrode à cavité”. The CME was described elsewhere.²⁷ In this case, the Ti_2C powder was mixed with the same conductive carbon black (Timcal Super C65) - in a 30 wt.% ratio to ensure good electrical contact - and manually pressed inside the microcavity.

All cells were assembled in an Ar-filled glove box (MBraun, $\text{O}_2 < 0.1$ ppm, $\text{H}_2\text{O} < 0.1$ ppm) to avoid any moisture contamination. Charge/discharge galvanostatic cycling and cyclic voltammetry tests were performed using a VMP3 cyler (Biologic, S.A.) at different C rates, considering 1 Li^+ exchanged per n hour at C/n .

Electrochemical in situ X-ray diffraction, XRD, patterns of the Ti_2C powder were collected on a Bruker D8 diffractometer using a $\text{Cu K}\alpha$ radiation ($\lambda = 1.5406 \text{ \AA}$) in the range $2\theta = 7\text{--}40^\circ$ with a step of 0.02° . The sample was placed in a Swagelok-type cell equipped with a beryllium window which also acted also as current collector, allowing in-situ XRD recording (cell from LRCS, Amiens University). The scans were recorded during a relaxation period in steps, every $y = 0.2$ (from $\text{Li}_y\text{Ti}_2\text{CO}_x$ in equation (2)), upon charge (reduction) and discharge (oxidation), using a rate of $C/10$.

Results and Discussion

Electrochemistry of the negative electrode: Ti_2C .— *Two-electrode cells.*— Figure 1 shows the cyclic voltammetry (CV) curves of Ti_2C and carbon black at $0.1 \text{ mV} \cdot \text{s}^{-1}$. To determine the contribution of carbon black to the total capacity of the film, currents are normalized to the same amount of C-black present in the Ti_2C :carbon black electrode. The Ti_2C material showed broad lithiation peaks at 1.8 V and 1.0 V and delithiation peak at 2.0 V both vs. Li^+/Li . The CV of the carbon black alone (dotted curve in Fig. 1) showed increased current, with no peaks, at potentials below 1.2 V vs. Li^+/Li . This is attributed to lithiation of the disordered structure of the carbon black in the electronically non-equivalent insertion sites. It is known that carbon blacks have a structure made of graphene sheets

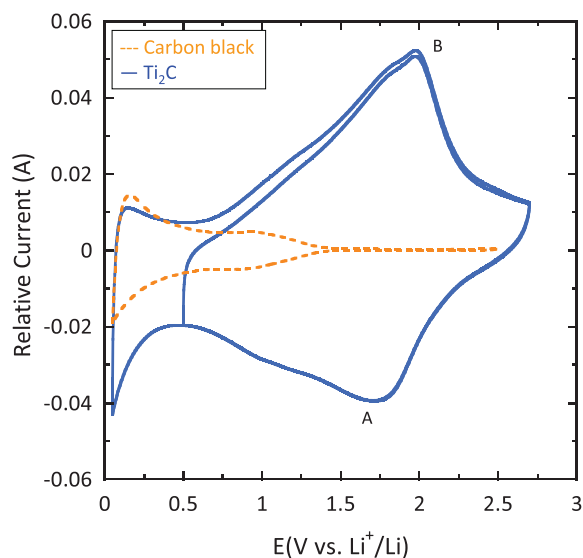


Figure 1. Cyclic voltammetry curves at $0.1 \text{ mV} \cdot \text{s}^{-1}$ of Ti_2C , and carbon black.

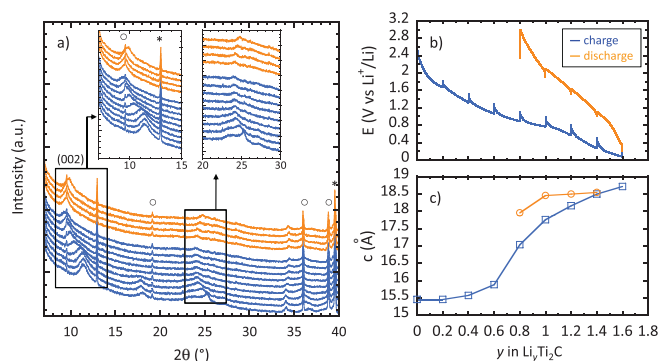


Figure 2. a) in-situ XRD patterns of Ti_2C collected every 0.2 Li^+ at a $C/10$ rate for charge (blue curves) and discharge (orange curves), *: unreacted Ti_2AlC , \circ : unreacted Ti_3AlC_2 , b) corresponding constant current charge/discharge curve, and c) c parameter calculated from (002) peak shift during charge and discharge.

and amorphous carbon, that lead to irreversible capacities and high rate performances.²⁸ Below 0.5 V vs. Li^+/Li , it is clear that no electrochemical faradaic reaction takes place in Ti_2C since most of the capacity measured can be attributed to the carbon black. Between 0.05 V and 2.7 V vs. Li^+/Li , the electrode capacity changes from $172 \text{ mAh} \cdot \text{g}^{-1}$ to $160 \text{ mAh} \cdot \text{g}^{-1}$. Since the difference comes from the carbon black, the capacity between 0.05 V and 0.5 V can be neglected. It follows that the reduction cutoff potential was set to 0.5 V vs. Li^+/Li .

The XRD patterns collected during a relaxation period every 0.2 Li^+ per unit formulae of Ti_2C are reported in Figure 2. Before cycling the pattern is characteristic of a multiphasic system including well-crystallized un-reacted Ti_2AlC and Ti_3AlC_2 together with a set of broad diffraction peaks that corresponds to exfoliated MXene based compound. During lithiation, the Bragg peaks position characteristic of un-reacted Ti_2AlC and Ti_3AlC_2 do not change, confirming that they are not electrochemically active. These peaks however, are useful as internal references for the determination of the positions of other peaks.

An examination of the XRD pattern shows that during the electrochemical process, no extra peaks appear; instead a reversible shift of the broad diffraction peaks is observed. This result is consistent with an insertion process occurring in the exfoliated MXene phases. A careful examination of the XRD pattern collected during Li insertion shows that the overall behavior can be divided into two domains. In the $0 < y < 0.4$ domain the main broad peak located at 11° is not affected, while, for example, the one located at 25° is shifted to lower diffraction angles. In the $0.6 < y < 1.4$ domain, the opposite is observed. The same observations can be made for other diffraction peaks indicating that the broad diffraction peaks probably correspond to the sum of two independent sets. Those two different sets may be related to different termination groups, e.g. O and F, involving different d_{hkl} lengths. The relative intensity of the two sets indicates that Ti_2C is the main phase; the minor phase has not yet been identified. As the domains are clearly separated, only the one corresponding to the electrochemical activity of Ti_2C is detailed.

During lithiation, the progressive downshift of (002) peak from $2\theta = 11.4^\circ$ to $2\theta = 9.4^\circ$ corresponds to an increase of c lattice parameter from 15.46 \AA to 18.72 \AA for Ti_2C (17.4% expansion). During delithiation the c parameter decreases down to 17.96 \AA , a value higher than the value obtained during lithiation for the same Li content (Fig. 2c). This can be related to the large irreversibility observed in the 1st cycle and interpreted by the trapping of Li^+ ions between the layers of MXene concomitant with SEI formation. Based on the XRD study it is reasonable to reach the following important conclusion: the charge storage in this Ti_2C -based material (plus an unidentified minor phase) is due to the intercalation of Li^+ ions and *not* due to a conversion reaction. This comment notwithstanding, more research is

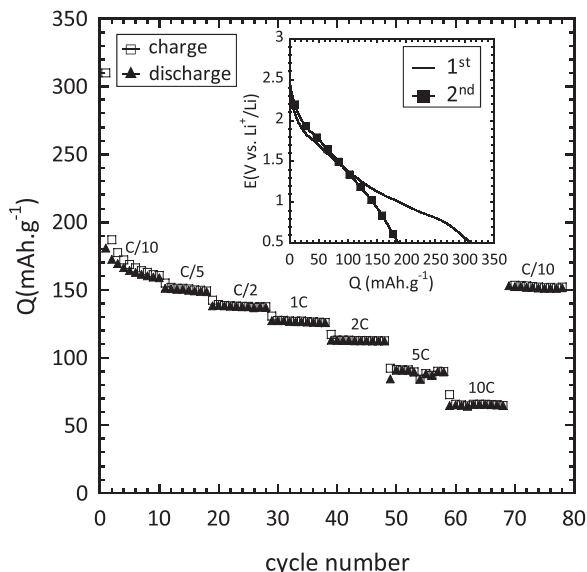


Figure 3. charge and discharge specific capacities of Ti_2C from C/10 to 10C rate. Inset shows the capacity loss between the 1st and 2nd galvanostatic charges.

needed and ongoing to further understand the details of the lithiation and delithiation mechanisms.

Figure 3 shows the dependencies of the galvanostatic charge and discharge capacities vs. cycle number between 0.5 V and 2.7 V vs. Li^+/Li as a function of different C-rates. As shown in the inset of Fig. 3, and consistent with the aforementioned conclusion, the material does not exhibit a flat faradaic plateau typical of a two-phase insertion process, meaning that lithiation and delithiation take place over a large range of potentials. This is consistent with the broad peaks observed in the diffractograms. Although the gradually inclined voltage profile might be considered as a drawback if this material is used as an anode in LIBs, it is worth investigating its behavior in an asymmetric EDLC as done here.

Another current drawback with the use of this material as an anode in LIB is the 40% irreversible capacity on the first cycle.²⁴ The latter is believed to be due to the SEI formation, in addition to, possibly, the partial irreversible trapping of Li^+ ions in the Ti_2C structure, as well as, some remaining surface functional groups such as hydroxides or fluorides present in the interlayer spaces of the 2-D structure. At

potentials below 1.0 V vs. Li^+/Li , SEI layers form.^{29,30} It is known that the SEI layer formation on carbonaceous anodes is of the highest importance in stabilizing the lithiation/delithiation process despite the Li^+ ions consumption by the electrolyte and there is no reason to believe that is not true here.

Electrochemical kinetics study of Li insertion in Ti_2C .—Cyclic voltammetry can be used to accurately distinguish between different insertion processes. The current, I (A), dependence on the potential scan rate, ν ($\text{V} \cdot \text{s}^{-1}$), are related according to:

$$I = a\nu^b \quad (3)$$

where a and b are adjustable parameters. In Eq. (3), the b -coefficient is related to the rate limiting step of the overall kinetics, i.e. whether the lithiation and delithiation reactions are diffusion-limited ($b = 0.5$) or not ($b = 1$).³¹

Figure 4a shows CV curves from $0.05 \text{ mV} \cdot \text{s}^{-1}$ to $5 \text{ mV} \cdot \text{s}^{-1}$. As noted above, two main lithiation and delithiation peaks are observed at 1.8 V and 2.0 V vs. Li^+/Li , labeled as peaks A and B, respectively. When the current dependencies are plotted vs. scan rate on a log scale (Fig. 4b), it is obvious that the relationship is linear with a slope of unity. In other words, $b = 1$, which, in turn, implies that Li^+ diffusion is *not* the limiting step of the overall electrochemical reaction kinetics.

When the capacity is plotted as a function of scan rate, again on a log-log plot (Fig. 4c) it is clear that the maximum capacity of $160 \text{ mAh} \cdot \text{g}^{-1}$ occurs at a scan rate of $0.05 \text{ mV} \cdot \text{s}^{-1}$ and is more or less constant up to $0.2 \text{ mV} \cdot \text{s}^{-1}$.

The inset in Fig. 4a shows the emergence of additional reductive and oxidative peaks at around 1.0 V at low scan rates, which can be attributed to different intercalation stages of Li^+ ions in the Ti_2C structure. Note that the signal at $5 \text{ mV} \cdot \text{s}^{-1}$ starts to be distorted due to ohmic losses, which limits the maximum scan rate to $5 \text{ mV} \cdot \text{s}^{-1}$.

Cavity microelectrode, CME.—CME is a convenient and efficient tool for qualitative kinetic analysis of various electroactive materials.^{32–35} The few micrograms of active material needed for measurements lead to low current and hence to small ohmic drops. This in turn allows electrochemical measurements over a wide range of scan rates. However, because the amount of material inserted inside the microcavity is not accurately known, the analysis from here on is qualitative.

Figure 5a shows cyclic voltammetry curves, obtained with a CME from $5 \text{ mV} \cdot \text{s}^{-1}$ to $100 \text{ mV} \cdot \text{s}^{-1}$. Note that the potential window was extended to 4.0 V vs. Li^+/Li to observe the complete oxidation reaction. The Ti_2C electrochemical signature is observed with the

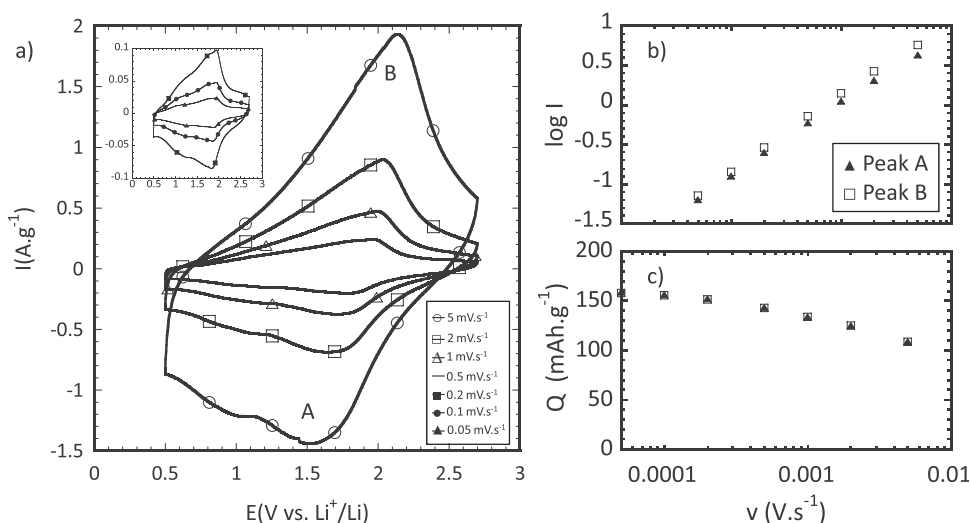


Figure 4. a) cyclic voltammetry curves from $0.05 \text{ mV} \cdot \text{s}^{-1}$ to $0.2 \text{ mV} \cdot \text{s}^{-1}$ (inset), and from $0.5 \text{ mV} \cdot \text{s}^{-1}$ to $5 \text{ mV} \cdot \text{s}^{-1}$, b) plot of peak current (in $\text{A} \cdot \text{g}^{-1}$) as a function of the potential scan rate, and c) specific capacity as a function of scan rate.

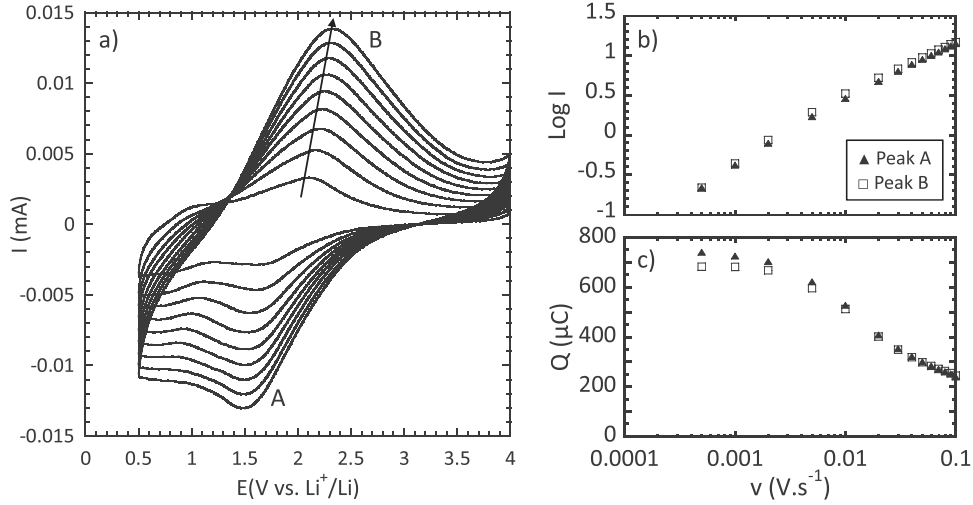


Figure 5. a) cyclic voltammograms obtained with a CME from $5 \text{ mV} \cdot \text{s}^{-1}$ to $100 \text{ mV} \cdot \text{s}^{-1}$, b) plot of peak current (in mA) as a function of the potential scan rate, and c) capacity as function of the potential scan rate.

peaks A and B at 1.8 V and 2.0 V vs. Li^+/Li during reduction and oxidation, respectively with a diffusion current plateau at potentials below 1.2 V vs. Li^+/Li during cathodic scans. As expected, the peaks broaden and the overpotential increases with increasing scan rates due to polarization effects (kinetic and ohmic).

When $\log I$ is plotted vs the $\log v$ (Fig. 5b), a change in slope is observed around $5 \text{ mV} \cdot \text{s}^{-1}$ for both anodic and cathodic scans. The calculated slopes, or b -coefficients, are listed in Table I. Confirming the conclusion reached above, it is again clear that the lithiation/delithiation of Ti_2C is not mass transport limited at rates below $5 \text{ mV} \cdot \text{s}^{-1}$. However, for v values higher than $5 \text{ mV} \cdot \text{s}^{-1}$, the b -coefficient decreases to around 0.7, implying that at the higher scan rates, mass transport in the bulk of the Ti_2C structure becomes important.

When the charge and discharge capacities are plotted as a function of $\log v$ (Fig. 5c), the maximum capacity is reached at scan rates below $2 \text{ mV} \cdot \text{s}^{-1}$, before decreasing at higher rates. The drop in capacity corresponds to the same scan rates at which the b -coefficients change. Those observations are consistent with the values obtained from the two-electrode cell measurements, even though the shapes of the electrochemical signals are different.

These results can be treated to a more sophisticated analysis. The total specific current is assumed to be the sum of two contributions: one part deriving from a diffusion-controlled process (I proportional to $v^{1/2}$), while the other from a capacitive-like charge storage process (I proportional to v). This assumption leads to:

$$Ip(V) = k_1 \cdot v + k_2 \cdot v^{1/2} \quad (4)$$

which can be rearranged to read:

$$Ip(V) \cdot v^{-1/2} = k_1 \cdot v^{1/2} + k_2 \quad (5)$$

where $Ip(V)$ is the current density at a given potential, k_1 and k_2 are coefficients, respectively, in $\mu\text{A} \cdot \text{V}^{-1} \cdot \text{s}$ and $\mu\text{A} \cdot \text{V}^{-1/2} \cdot \text{s}^{1/2}$, related to the relative contributions of the diffusion-controlled and capacitive-like parts to the total current as described elsewhere.³⁶ Plotting $Ip(V) \cdot v^{-1/2}$ vs. $v^{1/2}$ (Fig. 6) it is possible to determine both

k_1 and k_2 from the slopes and the y-intercepts, respectively. Note that both k_1 and k_2 are rate-dependent.

The non-diffusion limited contribution to the total current can be calculated assuming:

$$\%k_1(v) = k_1 \cdot v \cdot (k_1 \cdot v + k_2 \cdot v^{1/2})^{-1} \quad (6)$$

The inset in Fig. 6, plots the k_1 contribution to the total current, as a function of $\log v$. As expected, the trend is the same as the Q vs. $\log v$ plot shown in Fig. 5c, viz. showing a decrease in the k_1 contribution with increasing scan rates. This highlights once again that at the higher rates, mass transport limitation become important. Note that this contribution does not decrease to zero at high scan rates. Instead the $\%k_1$ reaches a steady value around 50% for both cathodic and anodic peaks. This phenomenon has already been observed in Ref. 27 and is attributed to contribution to the total current of the fast Li^+ ion redox reactions of the active sites located on the surface of the particles. In parallel, the capacity loss in the corresponding rate range reveals that these active sites become less accessible with increasing rates. Likely, the active surface layer becomes thinner. At

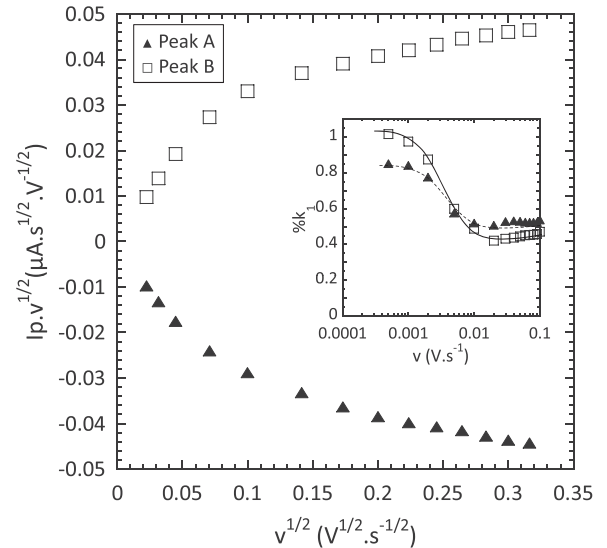


Figure 6. plot of $Ip \cdot v^{-1/2}$ vs. $v^{1/2}$ from $5 \text{ mV} \cdot \text{s}^{-1}$ to $100 \text{ mV} \cdot \text{s}^{-1}$. Inset: contribution of the non-diffusion limited current to the total current $\%k_1$ as a function of the potential scan rate.

Table I. b -coefficients obtained from Fig. 4 for anodic and cathodic peaks.

	$v < 0.5 \text{ mV} \cdot \text{s}^{-1}$	$v > 0.5 \text{ mV} \cdot \text{s}^{-1}$
Anodic peak (peak B)	0.95	0.65
Cathodic peak (peak A)	0.90	0.68

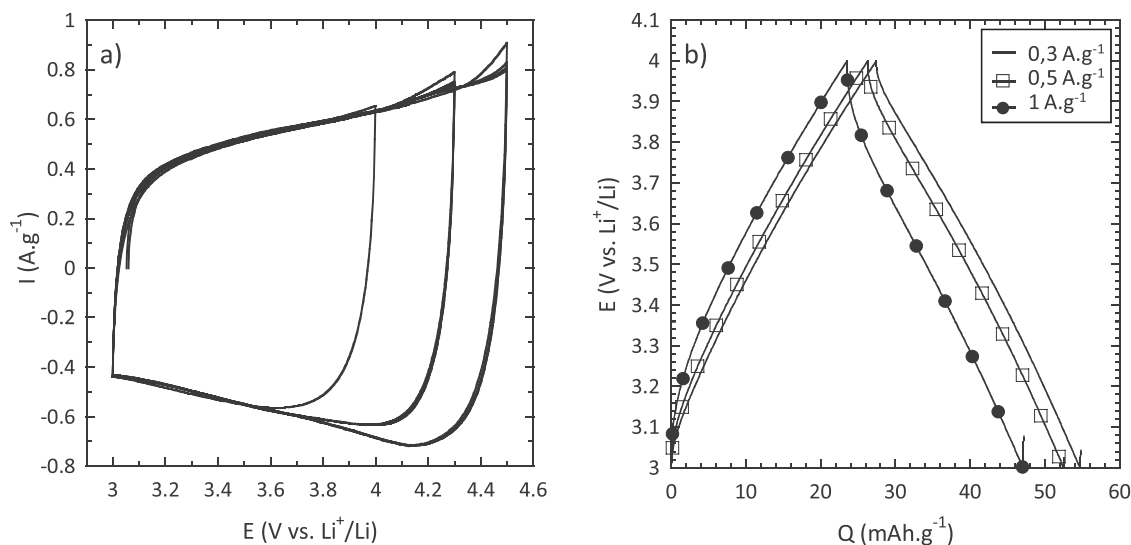


Figure 7. a) cyclic voltammograms at $5 \text{ mV} \cdot \text{s}^{-1}$ of a YP17 activated carbon in $1 \text{ M LiPF}_6 \text{ EC:DMC (1:1)}$ electrolyte with different voltage window, and b) constant current charge and discharge curves at $300 \text{ mA} \cdot \text{g}^{-1}$, $500 \text{ mA} \cdot \text{g}^{-1}$, and $1 \text{ A} \cdot \text{g}^{-1}$ between 3 V and 4 V vs. Li^+/Li .

rates below $5 \text{ mV} \cdot \text{s}^{-1}$, the k_1 values are 100% and 85% for anodic and cathodic processes, respectively (inset in Fig. 6). The differences in the rate limiting steps arise from faster electrochemical kinetics during oxidation than during reduction. Altogether, for both coin cells and the CME measurements, the Ti_2C material presents similar rate-dependence as a capacitive electrode up to $2\text{--}5 \text{ mV} \cdot \text{s}^{-1}$, meaning that no diffusion limitations are observed, allows fast Li^+ ions transport to the active sites and gives high rate capability.

Positive electrode: activated carbon YP17.— The capacities of activated carbon materials depend on the potential windows, ΔV , in which they are cycled, according to:

$$C(F/g) = Q(\text{mAh/g}) * 3600 / (\Delta V * 1000) \quad (7)$$

Figure 7 shows cyclic voltammetry and galvanostatic charge/discharge curves of YP17 in LP30 in different voltage ranges. It shows typical capacitive behavior and a capacitance of $100 \text{ F} \cdot \text{g}^{-1}$ at $300 \text{ mA} \cdot \text{g}^{-1}$ is obtained. As expected, the capacity increases as ΔV increases. However, the electrolyte oxidative stability limits the extension. Above 4.3 V vs. Li , the electrolyte starts oxidizing, which could result in a fade in cell capacity upon cycling. A capacity of $27 \text{ mAh} \cdot \text{g}^{-1}$ for YP17 between 3 V and 4 V vs. Li was calculated.

Ti_2C -YP17 asymmetric cell.— For the electrochemical study of an asymmetric cell, the positive and negative electrode masses must be balanced. The balance is based on the capacities of both materials. Here the Ti_2C negative electrode capacity at 1 C rate was chosen. The reason we focused on the higher rates, is to render them relevant for the performance of an asymmetric supercapacitor. Lower rates were thus not considered.

Since the capacity of the Ti_2C during the first cycle is $200 \text{ mAh} \cdot \text{g}^{-1}$ – including the $90 \text{ mAh} \cdot \text{g}^{-1}$ of irreversible capacity – between 3 V and 0.5 V vs. Li at 1 C rate, and the YP17 activated carbon capacity between 3.0 V and 4.0 V vs. Li is $27 \text{ mAh} \cdot \text{g}^{-1}$, the mass ratio of activated carbon to Ti_2C was fixed to 7.4. This ratio ensures that during the first charge, the activated carbon electrode and the negative electrode would cycle between 3.0 V and 4.0 V vs. Li and between 3.0 V and 0.5 V vs. Li^+/Li , respectively, giving a maximal cell voltage of 3.5 V . Taking into account that the irreversible capacity during the first cycle is 45% of the first charge capacity, the cell voltage discharge cutoff was fixed to 1.0 V . It is worth mentioning here that for these experiments the cell was cycled from 1.0 V to 3.5 V , and the positive and negative electrodes' potentials were recorded vs. the Li reference.

Galvanostatic charge-discharge cycling curves of the asymmetric cell are shown in Fig. 8, where the specific capacity is based on the Ti_2C weight. The first charge/discharge cycle (dotted line) shows capacity for SEI formation at the surface of the Ti_2C particles. The subsequent cycles show slight potential drift related to the irreversible capacity of Ti_2C , but stabilizes at $110 \text{ mAh} \cdot \text{g}^{-1}$ after 20 cycles. Considering the mass of both electrodes, the specific capacity of the device would be $14.2 \text{ mAh} \cdot \text{g}^{-1}$.

In order to characterize its power capability, the cell was then cycled from rates of 2 C to 20 C . As expected, the voltage window of the negative electrode increased with increased current densities. Indeed, a 20 C rate corresponds to $5 \text{ A} \cdot \text{g}^{-1}$ of Ti_2C , and $680 \text{ mA} \cdot \text{g}^{-1}$ of activated carbon, the latter becoming much more overcapacitive at such high current densities. As a result, the negative electrode operating voltage window increases from 0.5 V – 2.5 V to 0.3 V – 2.7 V vs. Li , as shown in the inset of Figure 8.

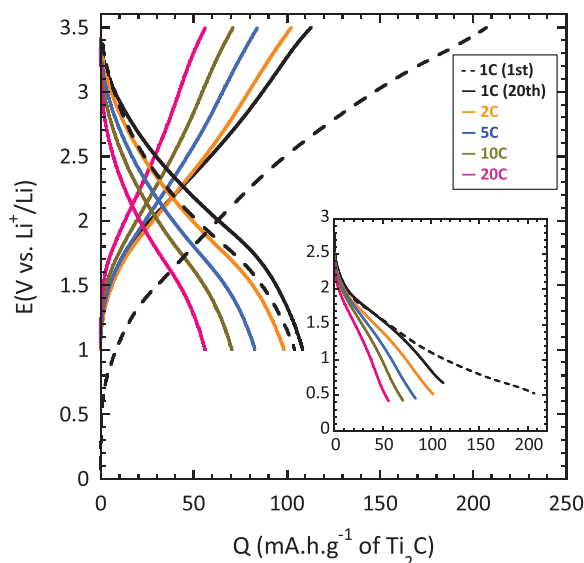


Figure 8. three-electrode constant current charge and discharge curves of a $\text{Ti}_2\text{C}/\text{YP17}$ asymmetric cell cycled between 3.5 V and 1.0 V from 1 C to 20 C rate. Specific capacity is represented based on the Ti_2C electrode. Inset: corresponding curves of the Ti_2C electrode.

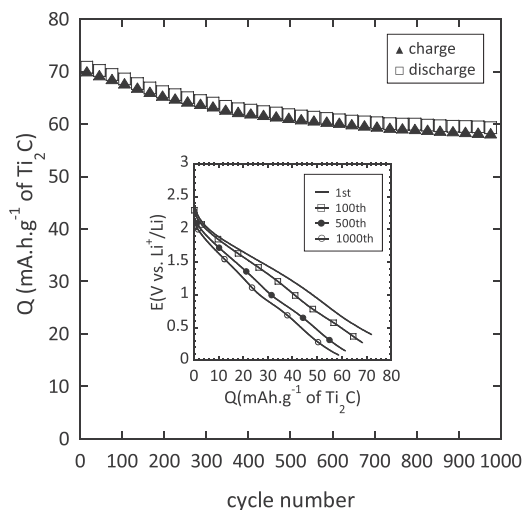


Figure 9. charge and discharge specific capacity vs. cycle number of a $\text{Ti}_2\text{C}/\text{YP17}$ asymmetric cell at 10C charge and 10C discharge with no relaxation between cycles. The capacity is based on the Ti_2C electrode. Inset: corresponding curves of Ti_2C electrode at different cycles showing the potential drift of the negative electrode.

The cell was subsequently charged and discharged at a rate of 10C, with no relaxation time between cycles. Figure 9 shows capacity vs. cycle number of the cell. The initial capacity was $70 \text{ mA} \cdot \text{h} \cdot \text{g}^{-1}$ based on the weight of Ti_2C , in accordance with previous values. After 1000 cycles, the capacity loss was $\sim 15\%$ at $60 \text{ mA} \cdot \text{h} \cdot \text{g}^{-1}$. The potential drift upon cycling was also found to be important, as it decreased to 0.1 V vs. Li at the end of charge after 1000 cycles, due to the intrinsic capacity loss of the material. Considering a maximum cell voltage of 3.5 V , the stored energy density was measured at to be $15 \text{ Wh} \cdot \text{kg}^{-1}$ of active materials (positive and negative) at $600 \text{ W} \cdot \text{kg}^{-1}$ after 1000 cycles. Given that the maximum energy and power densities are $50 \text{ Wh} \cdot \text{kg}^{-1}$ and $190 \text{ kW} \cdot \text{kg}^{-1}$, respectively, it follows that the Ti_2C -based material explored herein is suitable for use as an electrode in high energy-density supercapacitors.

Conclusions

Electrochemical lithiation and delithiation of Ti_2C were studied by in-situ XRD and electrochemical measurements. The c -parameter expansion confirmed that the Li^+ ions are inserted between the Ti_2C layers. The material exhibited a capacity of $65 \text{ mA} \cdot \text{h} \cdot \text{g}^{-1}$ at 10C rate despite a sizable irreversible capacity on the first cycle. Electrochemical kinetic analysis using both composite electrodes and a cavity microelectrode showed that no diffusion limitation at rates below $5 \text{ mV} \cdot \text{s}^{-1}$. This implies that up to that rate the Li^+ ions have easy access to the electroactive sites.

An asymmetric electrochemical cell was assembled and exhibited a maximum energy density of $30 \text{ Wh} \cdot \text{kg}^{-1}$ at $930 \text{ W} \cdot \text{kg}^{-1}$ of active materials for 1000 cycles. These results highlight the potential of using exfoliated MAX phases in devices in which high stable rates are required.

Acknowledgments

The authors thank the French network “CNRS MicroElectrode à Cavité” (MEC) for the kind supply of the CME and fruitful formation.

J.C. was supported by a French Délégation Générale pour l’Armement grant. This work has been done within the French network on electrochemical energy storage (RS2E). P.S thanks the FUI (“Récupérer” Project). The authors also thank Dr. M. Dolle (CEMES, UPR 8011) for the kind supply of the in-situ XRD cell. The work at Drexel University was supported by the Assistant Secretary for Energy Efficiency and Renewable Energy, Office of Vehicle Technologies of the U.S. Department of Energy under Contract No. DE-AC02-05CH11231, Subcontract 6951370 under the Batteries for Advanced Transportation Technologies (BATT) Program.

References

1. M. Armand and J.-M. Tarascon, *Nature*, **451**, 652 (2008).
2. T. Reddy (ed.), *Linden’s Handbook of Batteries*, 4th edition, McGraw-Hill, 2010.
3. B. E. Conway, *Electrochemical Supercapacitors: Scientific Fundamentals and Technological Applications*. (Kluwer, 1999).
4. P. Simon and Y. Gogotsi, *Nat. Mater.*, **7**, 845 (2008).
5. Y. Korenblit, M. Rose, E. Kockrick, L. Borchardt, A. Kvit, S. Kaskel, and G. Yushin, *ACS Nano*, **4**(3), 1337 (2010).
6. M. Arulepp, L. Permann, J. Leis, A. Perkson, K. Rumma, A. Jänes, and E. Lust, *J. Power Sources*, **133**, 320 (2004).
7. A. S. Arico, P. Bruce, B. Scrosati, J.-M. Tarascon, and W. V. Schalkwijk, *Nat. Mater.*, **4**(5), 366 (2005).
8. A. Kadjos, A. Kvit, F. Jones, J. Jagiello, and G. Yushin, *J. Am. Chem. Soc.*, **132**, 3252 (2010).
9. C. Largeot, C. Portet, J. Chmiola, P.-L. Taberna, Y. Gogotsi, and P. Simon, *J. Am. Chem. Soc.*, **130**, 2730 (2008).
10. R. Lin, P. Huang, J. Ségalini, C. Largeot, P.-L. Taberna, J. Chmiola, Y. Gogotsi, and P. Simon, *Electrochimica Acta*, **54**, 7025 (2009).
11. B. Daffos, P.-L. Taberna, Y. Gogotsi, and P. Simon, *Fuel Cells*, **10**(5), 819 (2010).
12. K. Naoi and P. Simon, *J. Electrochem. Soc.*, **17**, 34 (2008).
13. T. Brezesinski, J. Wang, S. H. Tolbert, and B. Dunn, *Nat. Mater.*, **9**, 146 (2010).
14. K. Brezesinski, J. Wang, J. Haetge, C. Reitz, S. O. Steinmueller, S. H. Tolbert, B. M. Smarsly, B. Dunn, and T. Brezesinski, *J. Am. Chem. Soc.*, **132**, 6982 (2010).
15. Z. Chen, V. Augustyn, J. Wen, Y. Zhang, M. Shen, B. Dunn, and Y. Lu, *Adv. Mater.*, **23**, 791 (2011).
16. A. Balducci, R. Dugas, P. L. Taberna, P. Simon, D. Pl’ee, M. Mastragostino, and S. Passerini, *J. Power Sources*, **165**, 922 (2007).
17. G. G. Amatucci, F. Badway, A. Du Pasquier, and T. Zheng, *J. Electrochem. Soc.*, **148**(8), A930 (2001).
18. JM Energy Corporation, <http://www.jmenergy.co.jp>.
19. K. Naoi, *Fuel cells*, **10**(5), 825 (2010).
20. T. Brousse, R. Marchand, P.-L. Taberna, and P. Simon, *J. Power Sources*, **158**, 571 (2006).
21. A. Balducci, W. A. Henderson, M. Mastragostino, S. Passerini, P. Simon, and F. Soavi, *Electrochimica Acta*, **50**, 2233 (2005).
22. M. Barsoum, *Prog. Solid State Chemistry*, **28**, 201 (2000).
23. M. Naguib, M. Kurtoglu, V. Presser, J. Lu, J. Niu, M. Heon, L. Hultman, Y. Gogotsi, and M. W. Barsoum, *Adv. Mater.*, **23**, 4248 (2011).
24. M. Naguib, J. Come, B. Dyatkin, V. Presser, P.-L. Taberna, P. Simon, M. Barsoum, and Y. Gogotsi, *Electrochem. Comm.*, **16**, 61 (2012).
25. M. Naguib, O. Mashtalir, J. Carle, V. Presser, J. Lu, L. Hultman, Y. Gogotsi, and M. W. Barsoum, *ACS Nano*, **6**, 1322 (2012).
26. C. Portet, P.-L. Taberna, P. Simon, and C. Laberty-Robert, *Electrochim. Acta*, **49**, 905 (2004).
27. J. Come, P.-L. Taberna, S. Hamelet, C. Masquelier, and P. Simon, *J. Electrochem. Soc.*, **158**(10), A1090 (2011).
28. M. Winter, J.-O. Besenhard, M. E. Pahr, and P. Novák, *Adv. Mater.*, **10**, 725 (1998).
29. F. Béguin and E. Frackowiak, (eds.) *Carbons for Electrochemical Energy Storage and Conversion Systems*, CRC Press, 2010.
30. W. A. Schalkwijk and B. Scrosati, *Advances in Lithium-ion batteries*, Springer, 2002.
31. A. J. Bard and L. R. Faulkner, *Electrochemical Methods: fundamentals and applications*, 2nd ed., John Wiley & Sons, New York (2001).
32. C. Portet, J. Chmiola, Y. Gogotsi, S. Park, and K. Lian, *Electrochim. Acta*, **53**, 7675 (2008).
33. V. Vivier, C. Cachet-Vivier, C. S. Cha, J.-Y. Nedelec, and L. T. Yu, *Electrochem. Comm.*, **2**(3), 180 (2000).
34. V. Vivier, C. Cachet-Vivier, B. L. Wu, C. S. Cha, J.-Y. Nedelec, and L. T. Yu, *Electrochem. Solid State Lett.*, **2**(8), 385 (1999).
35. C. Locatelli, A. Minguzzi, A. Vertova, P. Cava, and S. Rondonini, *Anal. Chem.*, **83**, 2819 (2011).
36. T. Brezesinski, J. Wang, J. Polleux, B. Dunn, and S. H. Tolbert, *J. Am. Chem. Soc.*, **131**, 1802 (2009).